ELSEVIER

Journal of Nuclear Materials 279 (2000) 57–64

journal of nuclear materials

www.elsevier.nl/locate/jnucmat

On the reactive occlusion of the (uranium trichloride + lithium chloride + potassium chloride) eutectic salt in zeolite 4A ☆

Dusan Lexa *, Leonard Leibowitz, Jeremy Kropf

Chemical Technology Division, Argonne National Laboratory, 9700 South Cass Avenue, Argonne, IL 60439, USA

Received 3 September 1999; accepted 17 November 1999

Abstract

The interaction between the (uranium trichloride + lithium chloride + potassium chloride) eutectic salt and zeolite 4A has been studied by temperature-resolved synchrotron powder X-ray diffraction, evolved gas analysis and differential scanning calorimetry, between 300 and 900 K. The onset of salt occlusion by the zeolite has been detected at 450 K. Evidence of a reaction between zeolitic water and uranium trichloride, leading to the formation of uranium dioxide, has appeared at 600 K. The uranium dioxide particle size increases from 2 nm at 600 K to 25 nm at 900 K – an indication of their extra-zeolitic location. No appreciable degradation of the zeolite structure has been observed.

1. Introduction

Glass–zeolite ceramic waste forms are being developed at Argonne National Laboratory for the disposal of radioactive waste salts from electrometallurgical treatment of spent nuclear reactor fuel [1,2]. The major component (70 wt%) of the process salt is the LiCl–KCl eutectic salt (58 mol% LiCl, 42 mol% KCl). In addition, the process salt contains at least 16 other fission product chloride and iodide salts and 2 mol% actinide chlorides, e.g., UCl_3, $NpCl_3$ and $PuCl_3$. As part of the waste treatment, the molten process salt is blended with zeolite 4A (10 wt% salt, 90 wt% zeolite), producing an occlusion compound with the salt residing inside the zeolite 4A cages. The presence of UCl_3 in the process salt, however, is a cause for concern. Because of the stability of uranium dioxide, UO_2, the potential exists for reaction between UCl_3 and both the zeolite 4A framework and the water contained therein. (Although the zeolite is aggressively dried prior to use, it still contains 0.1–1.0 wt% water.) Thermodynamic calculations indicate that both reactions are possible. Damage to the zeolite 4A framework could compromise its capability to retain the fission products. (Analogous reactions involving $NpCl_3$ and $PuCl_3$ are thermodynamically less favored.) Ex-situ powder X-ray diffraction examination of (salt + zeolite) samples heated up to 1000 K in an Ar atmosphere and quenched to room temperature indicated that UO_2 was, in fact, formed in the system at UCl_3 concentrations an order of magnitude higher than the UCl_3 process salt concentration. However, more detailed information, e.g., the identity of the UO_2-forming reaction, was needed. Hence, an investigation by differential scanning calorimetry (DSC), evolved gas analysis (EGA) and in-situ temperature-resolved synchrotron powder X-ray diffraction (XRD) was undertaken with the aim to better understand the nature and the extent of the interaction between UCl_3 and zeolite 4A.

2. Experimental

All chemicals were stored and manipulated inside a He atmosphere glove box (<1 ppm O_2, <1 ppm H_2O).

☆ Work supported by the US Department of Energy, Nuclear Energy Research and Development Program, under Contract W-31-109-Eng-38.

* Corresponding author. Tel.: +1-630 252 6747; fax: +1-630 972 4467.

E-mail address: lexa@cmt.anl.gov (D. Lexa).

0022-3115/00/$ - see front matter
PII: S0022-3115(99)00279-2

The UCl_3–LiCl–KCl eutectic salt (48.8 wt% U, 2.41 wt% Li, 6.57 wt% K, 0.02 wt% Ba, 0.01 wt% Na and Ce 0.02 wt%, all by ICP-AES and 0.02 wt% Cs by ICP-MS, corresponding roughly to 28.46 mol% UCl_3, 48.21 mol% LiCl and 23.23 mol% KCl), hereafter called salt, was produced by oxidizing U metal with $CdCl_2$ in a LiCl–KCl salt (66 mol% LiCl, 34 mol% KCl) [3]. Pieces of salt were pulverized in a laboratory mixer (1 min at 12 000 rpm) and the powder was transferred into a gas-tight glass container. The melting behavior of four salt samples was examined by DSC, see Fig. 1. A major melting peak with an extrapolated onset temperature of 685 K was observed. In addition, a minor, unresolved, melting peak was observed at 680 K most likely due to an impurity phase. The eutectic temperature has been reported as 691 ± 2 K for 30 mol% UCl_3–46 mol% LiCl–24 mol% KCl [4] and as 668 ± 2 K for 31.5 mol% UCl_3–38 mol% LiCl–30.5 mol% KCl [5]. A powder X-ray diffraction pattern of a salt sample indicated the presence of $K_3U_5Cl_{18}$ and LiCl. This is not consistent with the currently accepted UCl_3–LiCl–KCl phase diagram [4,5], which implies crystallization of UCl_3, LiCl and K_2UCl_5. Apparently, in addition to K_2UCl_5, there is another intermediate compound in the UCl_3–KCl system, the uranium-richer $K_3U_5Cl_{18}$. (There is evidence for an identical compound, $K_3La_5Cl_{18}$, in the $LaCl_3$–KCl system [6] and a similar compound, RbU_2Cl_7, in the UCl_3–RbCl system [7].)

Zeolite 4A, hereafter called zeolite, is an aluminosilicate with the overall formula $Na_{12}(AlSiO_4)_{12}$. The powder (no purity data, particle size <10 μm) was obtained from UOP (Des Plaines, IL). It was dehydrated at temperatures progressively increasing up to 798 K for 80 h, under flowing dry nitrogen, to less than 0.2 wt% H_2O (pyrolytic water weight loss) and stored in a gas-tight glass container. A powder X-ray diffraction pattern of a sample did not reveal the presence of any impurity phases.

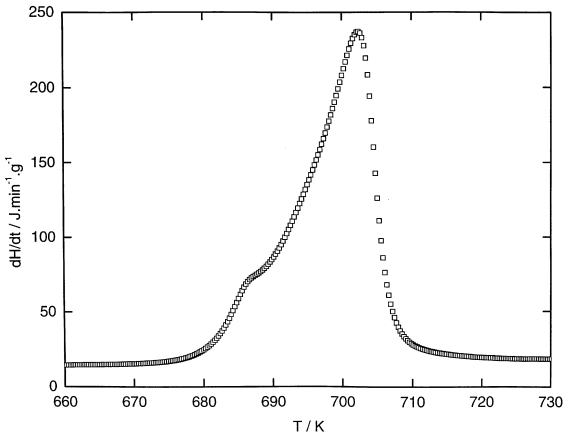

Fig. 1. DSC scan of the UCl_3–LiCl–KCl eutectic salt, 20 K min^{-1}.

Three (salt + zeolite) mixtures, hereafter called mixtures, with composition of 10.01, 20.04 and 30.14 wt% salt, were prepared by combining appropriate amounts of the component powders (±0.0001 g) in plastic vials. The vials were sealed with a cap and manually shaken for about 5 min to ensure homogeneity. In order to minimize possible solid-state interaction between the salt and the zeolite, no additional means of homogenization were employed. For reasons explained below (see Section 3), samples for DSC, EGA and XRD experiments, ~10 mg each, were taken mainly from the 30.14 wt% salt mixture.

DSC samples were transferred into weighed DSC pans (Perkin–Elmer, graphite, 6 mm i.d., graphite lid), lightly compacted, covered with lids, weighed and placed in sealable plastic containers for transfer to the DSC instrument. Samples were analyzed on a Perkin–Elmer model DSC-2C instrument with an attached dry box (<100 ppm H_2O) and ice–water bath cooling. Inside the dry box, the samples were transferred from the plastic containers into the measuring head in about 15 s. The sample and reference enclosures were each purged by ultra-high purity argon (99.999%) flowing at 20 cm^3 min^{-1}. Instrument control and data acquisition were fully computerized. Prior to this series of experiments, the baseline between $T = 298$ K and $T = 998$ K was optimized. The temperature scale was calibrated to ±0.5 K using In, Zn and K_2SO_4 melting temperature standards. By using the same three substances as enthalpy of fusion standards, a heat flow to signal calibration factor $\gamma = (4.37 \pm 0.05)$ J s^{-1} V^{-1} was obtained. Each experiment consisted of two runs with the same sample. Each run started with a 60 s isotherm at $T = 298$ K, followed by a 20 K min^{-1} ramp to $T = 898$ K and a 5 min isotherm at $T = 898$ K. The two runs were separated by a 160 K min^{-1} cool-down to $T = 298$ K and a 30 min equilibration period. The first run heat flow signal $(dH/dt)_1$ included contributions from the heat capacity of the sample and from thermal effects associated with the occlusion and reaction processes. The second run signal, $(dH/dt)_2$, only represented the sample heat capacity. Using a computerized version of a well-known procedure [8] to eliminate the effects of baseline drift, $(dH/dt)_2$ was subtracted from $(dH/dt)_1$ to yield dH/dt, the signal corrected for heat capacities. Assuming the applicability of the Neumann–Kopp rule, dH/dt represents the thermal effects associated with the occlusion and reaction processes only.

EGA samples were transferred into DSC pans (Perkin–Elmer, graphite, 6 mm i.d., no lid), lightly compacted and placed in sealable plastic containers for transfer to the EGA instrument. The instrument consists of an Ametek Dycor MA-200 quadrupole mass spectrometer operating at $\sim 10^{-8}$ Torr, attached to a resis-

tively heated Ta coil sample oven operating at $\sim 10^{-6}$ Torr. During transfer from the plastic container into the oven, samples had to be momentarily exposed to atmosphere. Each experiment consisted of a ramp from 300 to 825 K at 10 K min^{-1}. Gaseous species produced in the sample were escaping through a 1.6 mm diameter orifice in the Ni secondary cell directly toward the mass spectrometer electron-impact ionizer set at 70 V. The ionized species were directed into the quadrupole mass analyzer by a set of electrostatic focusing plates and further onto a Faraday cup detector. Instrument control and data acquisition were fully computerized. Changes in ion intensities associated with masses 2 (H_2), 14 (N_2), 18 (H_2O), 36 ($H^{35}Cl$) and 38 ($H^{37}Cl$) were monitored. No partial pressure calibration was performed as only relative changes of partial pressures of these species upon heating were sought.

XRD samples were transferred into weighed graphite pans [9] and lightly compacted. The pans were weighed and placed inside a Beryl/2 XRD enclosure, which is described in detail elswhere [9]. The sealed enclosure was removed from the glove box and transported to the Materials Research Collaborative Access Team insertion device (undulator A) beam line at Sector 10 at the Advanced Photon Source at Argonne National Laboratory. Experiments 'dfa', 'dfb', 'dfk' and 'dfl', each consisted of a single heating run starting with a 1 min isotherm at 300 K, followed by a temperature increase from 300 to 800 K at 10 K min^{-1} and a 10 min isotherm at 800 K. Experiment 'dfc' consisted of a single heating run starting with a 1 min isotherm at 300 K, followed by a temperature increase from 300 to 875 K at 20 K min^{-1} and an abrupt cool-down to 300 K (due to loss of sample temperature control). The X-ray energy, selected using a cryogenically cooled double-crystal Si (1 1 1) monochromator, was set to 11 keV ($\lambda = 0.11273$ nm). The Beryl/2 enclosure was mounted on an x–y motion stage and aligned to the center of an 8-circle Huber goniometer. Electrical and gas connections were made between the enclosure and the auxiliary systems. After final alignment, only the detector circle (2θ) was moved during the experiment, except for experiment 'dfk' which employed $\theta - 2\theta$ scanning. For the other scans the sample angle was fixed at 3° or 5°. The photon flux, measured by an ionization chamber behind the beam defining slit, was found to be $\sim 10^{11}$ s^{-1}. The X-ray wavelength was chosen to reduce the scan range, as well as avoid exciting Pt (sample cup) and U L-edge fluorescence X-rays, which would not be resolvable with a scintillation detector. Analyzer slits were used, rather than a crystal in order to maximize flux and simplify setup, at the expense of decreased resolution and increased background. 2θ scan speeds were 1.0° or 2.5° s^{-1}. The angular resolution (2θ) was measured to be between 0.04° and 0.12° for the various configurations (incident and analyzer slit sizes). The data acquisition system consisted of reading the ratemeter output with an analog–digital converter board installed in a PC. Small angle skewing resulted from this method of data collection, due to the 0.01 s time-constant on the ratemeter. Future improvements will include converting to pulse-counting electronics.

3. Theory and calculations

We have employed the HSC Chemistry for Windows 3.0 thermodynamic equilibrium calculation software package [10] to identify possible reactions in the UCl_3 + zeolite system. In the absence of zeolite thermodynamic data, we have used those available for nepheline, $NaAlSiO_4$, namely, 12 mol of $NaAlSiO_4$. In other work, we have observed that nepheline has occasionally formed when salt-free zeolite was heated above 823 K, indicating that the standard Gibbs free energy of formation of $Na_{12}(AlSiO_4)_{12}$ is less negative than that of 12 moles of $NaAlSiO_4$. The thermodynamically most favored reactions of $UCl_3 + H_2O$ and $UCl_3 + Na_{12}(AlSiO_4)_{12}$ are

$$4\,UCl_3 + 8\,H_2O(g) = 4\,UO_2 + 12\,HCl(g) + 2\,H_2(g), \quad (1)$$

$$4\,UCl_3 + Na_{12}(AlSiO_4)_{12} = 4\,UO_2 + Si + 11\,SiO_2 + 6\,Al_2O_3 + 12\,NaCl, \quad (2)$$

with standard reaction Gibbs free energies at 300 K equal to −270 kJ/mol and −710 kJ/mol, respectively and those at 800 K equal to −600 kJ/mol and −630 kJ/mol, respectively. While Eq. (1) represents the only feasible reaction of $UCl_3 + H_2O$ leading to UO_2, several reactions of $UCl_3 + Na_{12}$ $(AlSiO_4)_{12}$ leading to UO_2 can be envisioned, in addition to the reaction in Eq. (2). Analogous reactions leading to UOCl:

$$4\,UCl_3 + 8\,H_2O(g) = 4\,UOCl + 8\,HCl(g), \quad (3)$$

$$4\,UCl_3 + Na_{12}(AlSiO_4)_{12} = 4\,UOCl + 8\,SiO_2 + 4\,Al_2O_3 + 8\,NaCl \quad (4)$$

having standard reaction Gibbs free energies at 300 K equal to + 190 kJ/mol and −380 kJ/mol, respectively and those at 800 K equal to −70 kJ/mol and −330 kJ/mol, respectively, are thermodynamically less favored. It needs to be pointed out, however, that solid-phase kinetics might play an important role in determining which reactions will or will not be observed. Also, the openness of the system will favor reactions with gaseous products compared to reactions leading to solid products only.

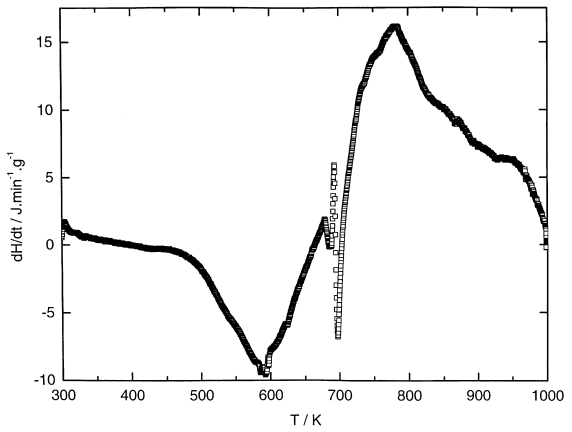

Fig. 2. DSC scan of the 30.14 wt% salt mixture, 20 K min^{-1}.

The UCl_3 content of the three mixtures prepared (10.01, 20.04 and 30.14 wt% salt) is such that, assuming a complete reaction with 0.2 wt% H_2O in the zeolite according to Eq. (1), 8%, 21% and 38%, respectively, of the zeolite could then react according to Eq. (2). In order to maximize the extent of the possible reaction between UCl_3 and zeolite and, thus, facilitate its detection, the 30.14 wt% salt mixture was used for most of the experiments.

XRD patterns obtained in experiments 'dfk' (24 patterns, 300–760 K) and 'dfl' (21 patterns, 300–700 K) were subjected to Rietveld refinements using the GSAS [11] software package. Crystallographic information on the four phases considered, i.e., zeolite 4A, $K_3U_5Cl_{18}$, UO_2 and graphite (sample pan) were obtained from literature [6,12,13]. Since the evaluation of the lattice parameter of zeolite 4A and of the particle size of UO_2, were the primary goals, the only refined parameters were phase scale factors, background coefficients, lattice parameters, profile coefficients, diffractometer zero and absorption [14].

4. Results and discussion

DSC: Five DSC experiments were performed with each of the three mixtures; all DSC scans exhibited identical features, irrespective of the mixture composition. A typical scan is shown in Fig. 2. At 450 K, the signal starts to negatively deviate from zero, suggesting an onset of an exothermic process that accelerates with increasing temperature. At 600 K, however, the exothermic character of the signal starts to abruptly diminish. While this may be due to the completion of the exothermic process and a return of the signal to zero, it is more likely caused by the onset of the endothermic process peaking at ~800 K and completed at 1000 K (especially considering that a linear extrapolation of the signal between 600 and 685 K to higher temperatures coincides with the signal between 725 and ~800 K). Interrupting the smooth character of this broad endothermic region is a sharp feature at 685 K. This feature was previously found [15] to represent the salt melting (endothermic) and the molten salt occlusion (exothermic) in (LiCl–KCl eutectic salt + zeolite) mixtures.

EGA: Eight EGA experiments were performed with the 30.14 wt% salt mixture, as well as four others with the zeolite only and one with the salt only. A typical EGA scan of the mixture is shown in Fig. 3. The broad H_2O peak between 300 and 600 K is due to desorption

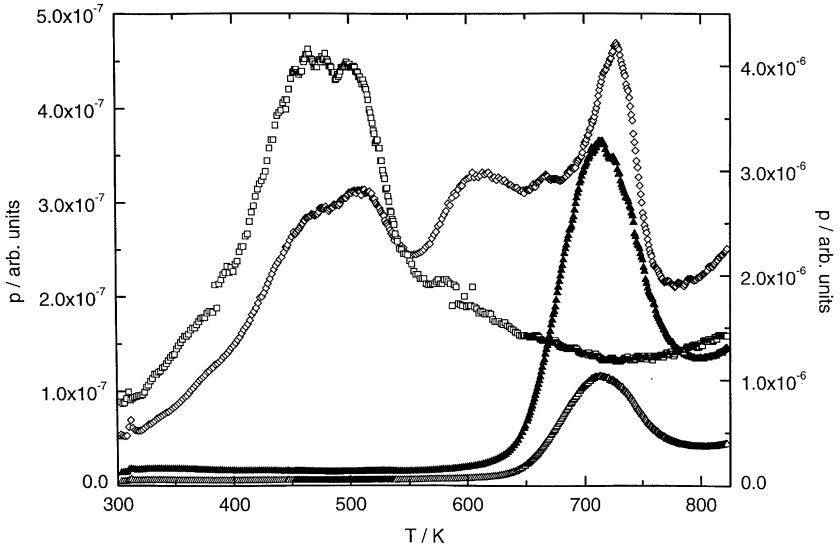

Fig. 3. EGA Scan of the 30.14 wt% salt mixture, 10 K min^{-1}, (◇) – H_2, (□) – H_2O, (▲) – $H^{35}Cl$, (△) – $H^{37}Cl$.

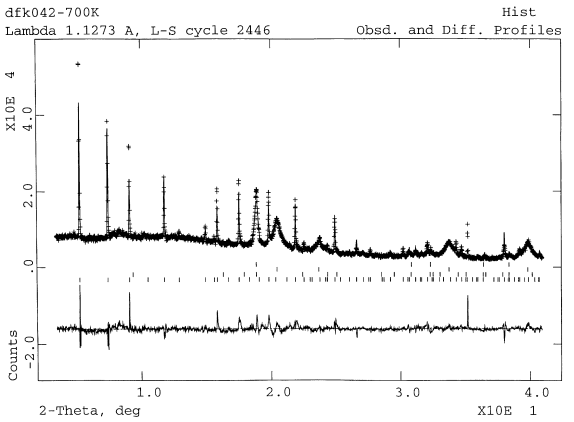

Fig. 4. Full range XRD pattern, 'dfk', 700 K. *Top*: observed (+), calculated (—); *Middle*: peak markers (top-to-bottom) graphite, UO_2, $K_3U_5Cl_{18}$, zeolite 4A; *Bottom*: difference curve.

of the H_2O adsorbed by the sample upon transfer into the oven. The coinciding H_2 peak was found to be caused by a reaction between the H_2O escaping from the sample and the Ta heating coil partially obscuring the mass spectrometer ionizer. Between 600 and 800 K, a peak in ion intensities of H_2, $H^{35}Cl$ and $H^{37}Cl$, respectively, is observed. (The $H^{35}Cl$ to $H^{37}Cl$ peak intensity ratio agrees well with the ^{35}Cl to ^{37}Cl natural abundance ratio of ~3.) Accordingly, assuming that a reaction involving UCl_3 and H_2O is taking place, the following equation might be written:

$$2\,UCl_3 + 4\,H_2O = 2\,UO_2 + 6\,HCl(g) + H_2(g). \qquad (5)$$

Similar peaks of H_2, $H^{35}Cl$ and $H^{37}Cl$ have not been observed in experiments with either the zeolite or the salt only.

XRD: Diffraction peaks in patterns obtained at the beginning of each experiment at 300 K were those of zeolite and salt – the mixture constituents. The absence of UO_2 diffraction peaks confirmed that the sample was not accidentally exposed to air upon transfer from the glove box to the beam line. In addition, the (0 0 2) diffraction peak of graphite at $2\theta = 19.2°$ appeared as a result of the X-ray beam striking the sample pan. This peak was present in all the patterns but did not in any way compromise the analysis. A typical diffraction pattern is shown in Fig. 4 together with a pattern obtained from the Rietveld refinement ($R_{wp} = 0.1$[11]) and a difference curve.

4.1. Formation of UO_2

In every set of XRD patterns, diffraction peaks of uranium dioxide, UO_2, first observed at 600 K and increasing in intensity with increasing temperature, were the most prominent feature. The evolution of the (1 1 1) diffraction peak of UO_2 in experiment 'dfc' is shown in Fig. 5. Its parameters, including peak position, $2\theta_0(T)$ and integral width, $B(T)$, have been determined by a computerized least-squares fit of the last 14 sets of data

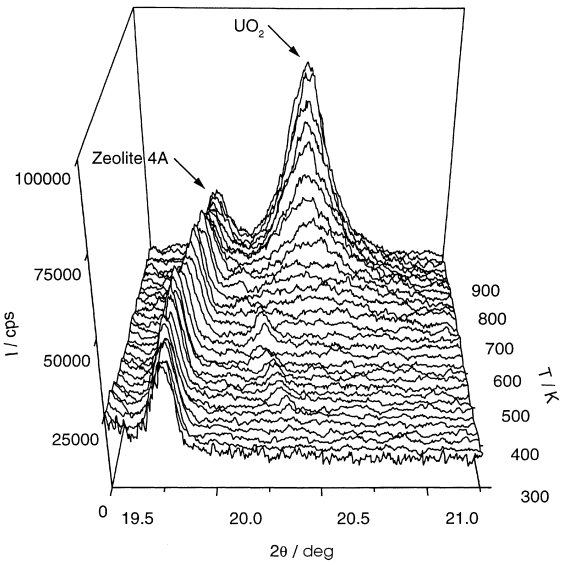

Fig. 5. UO_2 formation and Zeolite 4A lattice contraction by XRD.

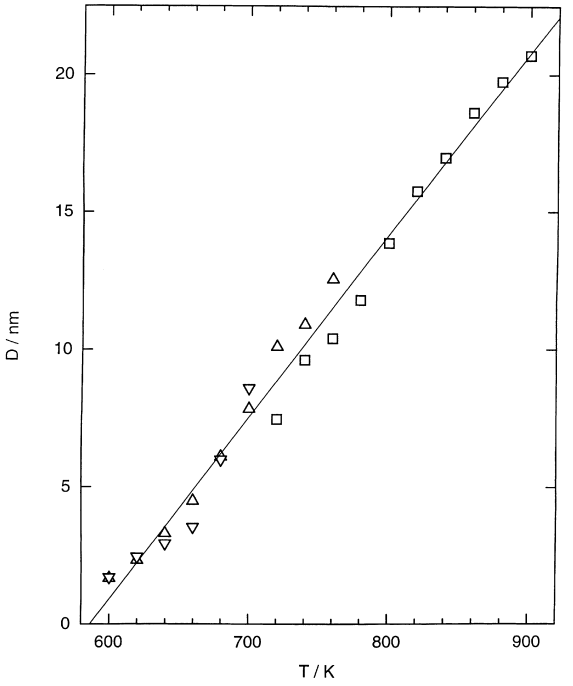

Fig. 6. UO_2 particle growth from XRD, (□) – 'dfc', 20 K min^{-1}, (△) – 'dfk', 10 K min^{-1}, (▽) – 'dfl', 10 K min^{-1}.

(640–900 K) between $2\theta = 20.00°$ and $2\theta = 21.00°$ to a Gaussian profile. Without a clear trend in $2\theta_0(T)$, the last 10 results (720–900 K) have been averaged to yield a value of $2\theta_0 = 20.47 \pm 0.01°$, corresponding to a UO_2 cubic cell parameter of $a = 0.5493 \pm 0.0003$ nm. For experiments 'dfk' (600–740 K) and 'dfl' (600–680 K) the Rietveld refinement yielded $a = 0.5496 \pm 0.0016$ nm and $a = 0.5481 \pm 0.0054$ nm, respectively. These numbers agree rather well with the literature [13] value of $a = 0.5467$ nm at room temperature. The integral widths of the (1 1 1) diffraction peak of UO_2 in experiment 'dfc', ranging roughly from 0.3° to 0.9°, have been used to calculate the mean UO_2 crystallite size, $D(T)$, defined as the cube root of the crystallite volume, via the Scherrer equation [16]. The pure diffraction line broadening, $\beta(T)$, has been replaced by $B(T)$, since, for Gaussian profiles, they are connected with each other via [16] $B^2 = \beta^2 + b^2$. The term b^2 (0.01), the square of the instrumental line broadening, can be neglected versus B^2 (0.1–1). The mean UO_2 crystallite size as a function of temperature is plotted in Fig. 6 together with results of the Rietveld refinement for experiments 'dfk' and 'dfl'. Assuming a constant growth rate, δ, a least-squares fit yielded a value of $\delta = 0.066 \pm 0.002$ nm K^{-1}. (A growth rate thus defined is expected to diminish with increasing heat rates; however, no discernible differences were observed between the 20 K min^{-1} 'dfc' and the 10 K min^{-1} 'dfk' and 'dfl' data.) It is seen that UO_2 formation starts just below 600 K. The UO_2 crystallite size increasing from 2 nm at 600 K to 20 nm at 900 K suggests that the observed UO_2 crystallites are located outside the zeolite lattice. (The diameter of the α- and β-cage of zeolite is 1.14 and 0.66 nm, respectively [17].)

4.2. Zeolite lattice contraction

Zeolite lattice parameters from experiment 'dfc' are averages calculated from the positions of eight of the most intense zeolite peaks in the diffraction pattern from $2\theta = 5.2°$ to $2\theta = 38.0°$, while those for experiments 'dfk' and 'dfl' are results of a Rietveld refinement. The zeolite lattice parameter at 300 K is $a = 2.453 \pm 0.001$ nm, $a = 2.4594 \pm 0.0002$ nm and $a = 2.4585 \pm 0.0003$ nm, respectively. These numbers are in excellent agreement with the literature [12] value of $a = 2.4555$ nm. The results of the zeolite lattice parameter evaluation as a function of temperature (in the form of expansion, $\Delta a/a$) are given in Fig. 7. It is seen that, at temperatures below 450 K, the zeolite lattice expands with increasing temperature. The coefficient of thermal expansion determined as the slope of the expansion curve between 300 and 400 K as 12.9×10^{-6} K^{-1} from experiment 'dfc' is rather large, but the values of 5.9×10^{-6} and 6.2×10^{-6} K^{-1} obtained from experiments 'dfk' and 'dfl', respectively, are in good agreement with the previously measured value

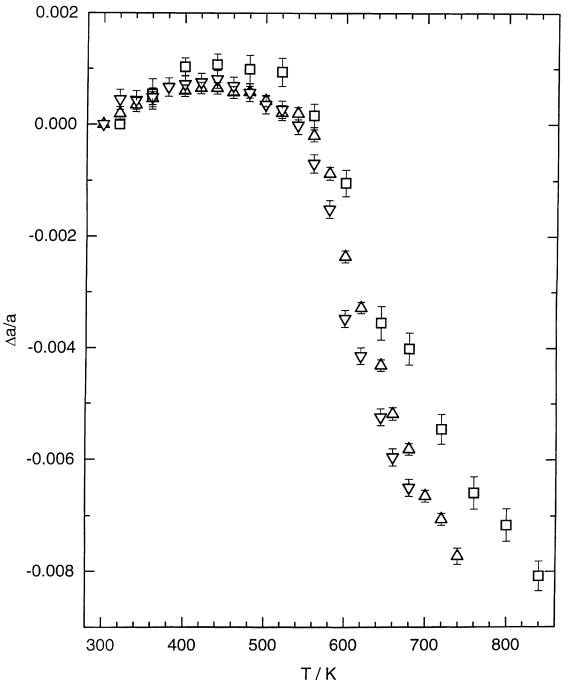

Fig. 7. Zeolite 4A thermal and chemical expansion from XRD, (□) – 'dfc', 20 K min^{-1}, (△) – 'dfk', 10 K min^{-1}, (▽) – 'dfl', 10 K min^{-1}.

[18] of 6.29×10^{-6} K^{-1}. Above 450 K, however, the zeolite lattice contraction becomes apparent. An example of the small changes in the position of the zeolite peaks can be seen in Fig. 5 at $2\theta = 19.5°$. It has been observed previously [19] that the zeolite lattice contracts upon molten salt occlusion. Since the UCl_3–LiCl–KCl eutectic salt does not melt until 685 K, some form of solid-state transport, e.g., solid-state diffusion, of the salt into the zeolite lattice is implicated below that temperature.

No XRD evidence of zeolite 4A decomposition products according to Eq. (2) such as Si, SiO_2, Al_2O_3 and NaCl was found. Trace amounts of what could be uranium disilicide, USi_2, were detected in the 'dfa' and 'dfb' experiments between 600 and 800 K. The decrease in the intensity of zeolite 4A diffraction peaks, originally thought to be a sign of the zeolite 4A lattice destruction, has since been observed in analogous experiments with (LiCl–KCl eutectic salt + zeolite) mixtures [20] and is, hence, a result of non-reactive salt occlusion.

4.3. Transformation $K_3U_5Cl_{18} \rightarrow K_2UCl_5$

A transformation of the uranium-rich $K_3U_5Cl_{18}$ salt, present in the starting mixture, into the uranium-poor K_2UCl_5 salt has been observed. This is shown in Fig. 8 ('dfb'), where the (1 0 0) diffraction peak at 2θ of

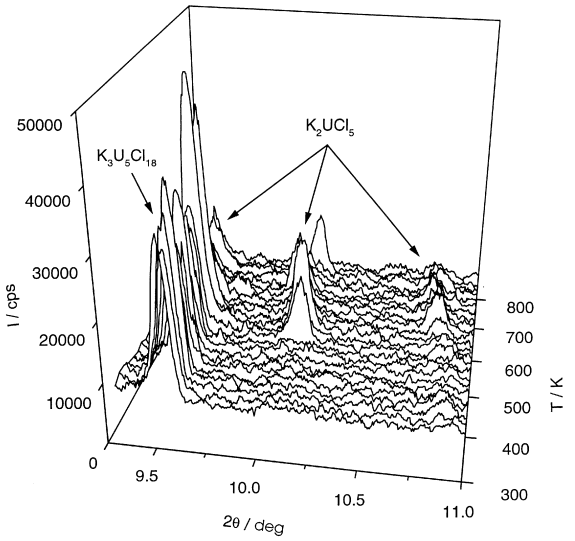

Fig. 8. Transformation of $K_3U_5Cl_{18}$ into K_2UCl_5 by XRD.

9.5°, associated with $K_3U_5Cl_{18}$, is being replaced by a set of (1 0 1), (2 0 0) and (0 1 1) peaks at 2θ of 9.5°, 10.1° and 10.9°, respectively, associated with K_2UCl_5. The transformation starts at 600 K and K_2UCl_5 peaks are still present at 800 K. Accordingly, the following equation might be written:

$$2\,K_3U_5Cl_{18} = 3\,K_2UCl_5 + 7\,UCl_3. \quad (6)$$

The UCl_3 formed in this reaction becomes available for a subsequent reaction with the zeolite.

5. Conclusions

Combining the information obtained by DSC, EGA and XRD, it is possible to propose the following sequence of events taking place in the (UCl_3–LiCl–KCl eutectic salt + zeolite 4A) mixture upon heating from room temperature. Between 300 and 450 K, no chemical changes occur. At 450 K, the LiCl and/or the KCl start diffusing into the zeolite 4A lattice forming an occlusion compound. This process is exothermic and results in a significant zeolite 4A lattice contraction. At 600 K, continuing LiCl and/or KCl occlusion leads to the expulsion of the zeolitic H_2O (<0.2 wt%) from the zeolite 4A lattice, which reacts with $K_3U_5Cl_{18}$ in the UCl_3–LiCl–KCl eutectic salt

$$8/7\,K_3U_5Cl_{18} + 8H_2O = 12/7\,K_2UCl_5 + 4\,UO_2 + 12\,HCl(g) + 2\,H_2(g). \quad (7)$$

This process is endothermic. The UO_2 crystallites being formed increase in size form 2 nm at 600 K to 20 nm at 900 K. At 685 K, the UCl_3–LiCl–KCl eutectic salt melts and is occluded by the zeolite 4A.

No zeolite 4A decomposition products were observed. Hence, it is concluded that the UCl_3 in the UCl_3–LiCl–KCl eutectic salt does not react with the zeolite 4A to any appreciable extent. However, thermodynamically-spontaneous reactions between UCl_3 and zeolite 4A have been identified. This discrepancy, explainable by sluggish kinetics or inaccurate thermodynamic data, will require further study. Since the UCl_3/zeolite 4A ratio in the production of the glass–zeolite waste form is significantly lower than the one used in this work, the H_2O present in the dehydrated zeolite 4A is expected to react with all the UCl_3 from the process salt to form UO_2. Hence, the presence of UCl_3 in the process salt should not have any adverse affects on the performance of the glass–zeolite waste form.

Acknowledgements

Use of the Advanced Photon Source was supported by the US Department of Energy, Basic Energy Sciences, Office of Science (DOE-BES-SC), under Contract No. W-31-109-Eng-38. The MRCAT beam lines are supported by the member institutions and the US DOE-BES-SC under Contracts DE-FG02-94ER45525 and DE-FG02-96ER45589.

References

[1] C. Pereira, M. Hash, M. Lewis, M. Richmann, JOM 49 (7) (1997) 34.
[2] M.A. Lewis, D.F. Fischer, L.J. Smith, J. Am. Ceram. Soc. 76 (11) (1993) 2826.
[3] Z. Tomczuk, personal communication, Argonne National Laboratory, 1998.
[4] B.J. Thamer, Los Alamos National Laboratory Report, LA 3579-MS, Los Alamos, 1966.
[5] V.N. Desyatnik, B.V. Dubinin, Zh. Priklad. Khim. 48 (4) (1975) 885.
[6] H.J. Seifert, H. Fink, G. Thiel, J. Less-Common Met. 110 (1985) 139.
[7] I.G. Suglobova, D.E. Chirkst, Koordinat. Khim. 7 (1) (1981) 97.
[8] M.J. Richardson, in: K.D. Maglic, A. Ceazairliyan, V.E. Peletsky (Eds.), Compendium of Thermophysical Property Measurement Method, vol. 1, Plenum, New York, 1984, p. 676.
[9] D. Lexa, Rev. Sci. Instrum. 70 (5) (1999) 2242.
[10] HSC Chemistry for Windows 3.0, Outokumpu Research Oy Pori, Finland, 1997.
[11] A.C. Larson, R.B. Von Dreele, GSAS-General Structure Analysis System, Los Alamos National Laboratory Report LA-UR-86-748, 1987.
[12] J.J. Pluth, J.V. Smith, J. Am. Chem. Soc. 102 (1980) 4704.

[13] PDF File, International Center for Diffraction Data, Newtown Square, PA, 1998.
[14] J.E. Post, D.L. Bish, in: J.E. Post, D.L. Bish (Eds.), Reviews in Mineralogy, Modern Powder Diffraction, vol. 20, The Mineralogical Society of America, Washington, DC, 1989, p. 287.
[15] D. Lexa, J. Chem. Thermodyn. 31 (1999) 811.
[16] H.P. Klug, L.E. Alexander, X-ray Diffraction Procedures for Polycrystalline and Amorphous Materials, Wiley, New York, 1954, p. 491.
[17] D.W. Breck, Zeolite Molecular Sieves, Wiley, New York, 1974, p. 84.
[18] R.E. Taylor, H. Groot, J. Ferrier, D.L. Taylor, Thermophysical Properties Research Laboratory Report 1697, Purdue University Research Park, 1996.
[19] C. Pereira, personal communication, Argonne National Laboratory, 1998.
[20] D. Lexa, L. Leibowitz, A.J. Kropf (in preparation).